Received: 22 November 2023 | Revised: 20 March 2024 | Accepted: 25 June 2024

DOI: 10.1002/suco.202301022

ARTICLE

fib CEB-FIP WILEY

Effect of high temperature on FRCM-confined concrete

Klajdi Toska[1,2] | **Flora Faleschini**[3] | **Anne-Lise Beaucour**[1] | **Carlo Pellegrino**[3] | **Albert Noumowe**[1]

[1]Laboratoire de Mécanique & Matériaux du Génie Civil – L2MGC, CY Cergy Paris Université, Neuville-sur-Oise, France

[2]CY Institute for Advanced Studies, Neuville-sur-Oise, France

[3]Department of Civil, Environmental and Architectural Engineering, University of Padova, Padova, Italy

Correspondence
Klajdi Toska, Laboratoire de Mécanique & Matériaux du Génie Civil – L2MGC, CY Cergy Paris Université, 5 Mail Gay Lussac, 95000 Neuville-sur-Oise, France.
Email: klajdi.toska@cyu.fr

Funding information
H2020 Marie Skłodowska-Curie Actions, Grant/Award Number: 945380

Abstract

The paper investigates the effect of high temperature exposure on the performance of concrete confined through textile/fabric-reinforced composites. Small-scale cylindrical specimens (150 × 300 mm) were confined using two types of carbon fibers (dry and epoxy-resin coated). For the sake of comparison, two confining layers were applied to all specimens. After curing, cylinders were exposed to four ranges of increasing temperatures—being 20°C (ambient), 80°C, 100°C, and 250°C and, after cooling down, were tested under compressive cyclic loading. The experimental results show that thermal stress significantly influences the confinement effectiveness of textile-reinforced composites. Exposure to high temperatures reduces the ultimate confined strength and significantly influences the overall axial stress–strain behavior.

KEYWORDS

concrete confinement, FRCM, high temperature, model prediction, TRM

1 | INTRODUCTION

As addressing sustainability issues becomes more and more important for the construction industry, one of the most effective ways to tackle the topic and reach the sustainability goals defined by Reference 1 remains retrofitting and upgrading existing structures, to extend their service life and avoid demolition as well as reconstruction interventions. In this regard, composite materials have played an important role in structural engineering to strengthen and repair under-designed or damaged existing concrete or masonry structures. Among others, textile or fabric-reinforced composites (known also as textile-reinforced concrete [TRC], textile-reinforced mortar [TRM], or fabric-reinforced cementitious matrix [FRCM]) are becoming gradually more and more popular at the expense of the use of the more traditional fiber-reinforced polymers (FRPs). Even though FRPs show a better performance in terms of tensile strength and retrofitting effectiveness,[2] textile-reinforced cementitious composites have a higher compatibility with existing concrete and masonry structures and outperform the former in terms of durability.[3,4] Due to the inorganic matrix used in place of the polymer resins of the FRPs, FRCM composites are also easier to be applied on irregular surfaces,[5] show a better behavior at high temperatures[6,7] and have enhanced physical–chemical compatibility with existing substrates.[2]

Among the retrofitting techniques employed with composite materials, confinement of concrete columns through external jacketing is one of the most used, especially on seismically prone areas. Bournas et al.[8] investigated the effectiveness of confinement interventions through FRP and TRM jackets. The results showed that

TRM is about 10% less effective in terms of compressive strength enhancement compared to FRP jacketing. However, when the seismic performance of RC columns was investigated through horizontal lateral loading, the difference between columns confined with FRP and TRM jackets was very limited. Recently, some of the authors experimentally investigated the behavior of FRCM-confined concrete under compressive cyclic loading and the influence that different parameters, such as overlapping length, fabric equivalent thickness, fibers coating and coating type, etc., have on the confinement effectiveness of FRCM jackets.[9,10] Furthermore, textile-reinforced composites have been also proven able to repair damaged reinforced concrete columns due to excessive axial loading[11] and to enhance the seismic performance of both undamaged and damaged real-scale columns, as well as beam-column joints.[12–15]

Among hazards that a structure may face during their service life, fire events can significantly influence the construction material properties and, therefore, the overall structural safety. FRP composites have a poor fire behavior due to the low glass transition temperature of the polymeric matrix, hence, composites based on a cementitious matrix generally show a better resistance to high temperature exposure. However, cementitious composites are relatively recent and further research is still needed to understand the effect of high temperatures on their behavior and on the effectiveness of the retrofitting techniques in which these materials are applied when exposed to high thermal stresses.

Regarding concrete materials, several research have been conducted over time to investigate their behavior when exposed to high temperatures. However, predicting the mechanical properties variation after fire events remains a complicated issue since concrete is a heterogeneous material and its behavior at high temperature depends on many parameters, such as: type and amount of cement paste,[16] presence of free and bound water,[17,18] aggregates nature,[19–21] presence and type of fibers,[22,23] initial compressive strength,[23,24] etc.

When considering textile-reinforced cementitious composites, their behavior at high temperature depends not only on the cementitious matrix itself, but also on the effect that the temperature has on the reinforcement as well as on the textile-to-matrix interface. The importance of thermal actions on textile-reinforced composites is highlighted also by the recent Italian guidelines on the qualification of these composite materials, which require an investigation on the high temperature behavior before the material can receive its certification.[25] The temperature effect on the tensile strength of FRCM and FRP composites was investigated by References 26 and 27. The test results showed a good behavior of the FRCM coupons even though the residual tensile strength tends to decrease as the exposure temperature increases. The behavior of alkali-resistant glass textile embedded in a cementitious matrix was investigated by Reference 28 both in terms of residual strength and through a thermo-mechanical test. The authors observed a positive effect of the temperature up to 150°C and then a gradual decrease for temperature between 150 and 600°C. In Reference 29, the authors investigated the effect of short discontinuous fibers added in the matrix on the thermal-mechanical behavior of TRC. Recently, Kapsalis et al.[30] investigated the effect of fire exposure on TRC specimens. The experimental campaign considered different textile materials (carbon and glass), both coated and uncoated conditions and temperature exposure up to 700°C. The residual properties of the specimens were tested under uniaxial tensile loading and the results showed that TRC with uncoated carbon fibers maintained the highest residual capacity after fire exposure. Regarding the bond behavior of textile-reinforced specimens the experimental work carried out by de Andrade Silva et al.[31] should be mentioned. Coated and uncoated carbon yarns were tested under a double-sided pullout test configuration after being subjected to a heating regime at temperatures of 20, 100, 150, 200, 400, and 600°C. The results showed an improvement of the bond strength for temperatures below 200°C for the coated yarns while for temperatures above 400°C the residual strength was significantly reduced. Recently, Bertolli et al.[32] investigated the bond behavior of carbon FRCM applied to masonry substrate and exposed to thermal preconditioning up to 300°C for about 4 h. The results showed that the polymeric impregnation improved the mechanical properties of the FRCM even after high temperature exposure. An extensive review on the experimental research on the high temperature behavior of textile-reinforced composites can be found at Reference 33.

However, regarding confinement interventions, the behavior of FRCM-confined concrete subjected to high temperature is still little investigated in the existing literature. Trapko[34] analyzed the effect of high temperature exposure on the confinement effectiveness of FRCM composites and compared them to that of FRPs. Note that in this work the range of investigated temperatures was limited to only 80°C. More recently, Ombres[35] and Ombres et al.[36] experimentally investigated the effect of thermal conditioning on concrete confined through PBO (phenylene-benzobisoxazole) FRCM composites. The campaign investigated temperatures up to 250°C and the results showed that the high temperature exposure affected both the mechanical strength of the FRCM material and the effectiveness of the PBO-FRCM jacket to confine the concrete specimens. Cerniauskas et al.[37] analyzed the

effectiveness of FRP and TRM confining systems exposed up to temperatures of 400°C. The results showed that the effectiveness of the FRP jackets bonded with epoxy decreased considerably, but did not vanish, with increasing temperatures, while, TRM confining system, bonded with inorganic mortar, demonstrated a better performance than the FRP confining systems. TRM-confined specimens showed an initial slight strength reduction for temperatures between 100 and 200°C while an enhanced strength was observed at 400°C. Reference 38 investigated concrete cylinders with different compressive strengths, confined with one or two FRCM layers, and subjected to target temperatures of 100, 400, and 800°C. Specimens exposed to 100°C exhibited a slight increase in their compressive strength, cylinders heated to 400°C showed no particular trend while specimens heated up to 800°C experienced a significant strength reduction.

It is clear that the actual state of the art on the topic is still very poor and the results presented, even though very promising, are often in conflict with each other. In this context, the goal of the present study is to investigate the performance of FRCM-confined concrete subject to increasing temperature levels, varying from ambient to 250°C. Cylindrical specimens were cast using the same concrete batch and, after curing, were confined through FRCM jackets. Two types of carbon fabric were used in the FRCM composites: dry and epoxy-resin (ER) coated. Reference and confined specimens were subjected to cyclic compressive loading and the experimental results were then compared with predictions deriving from existing guidelines and confinement models present in the literature.

2 | MATERIALS AND METHODS

2.1 | Specimens' features

The present experimental campaign investigates the behavior of FRCM-confined concrete when subjected to temperatures up to 250°C. Two types of carbon fabric were used for the FRCM composite, dry (uncoated) and ER coated ones. A total of 23, small-scale, cylindrical specimens with diameter and height, $d \times h = 150 \times 300$ mm, were tested during the experimental campaign. Specimens are labeled with a nomenclature that consists of three parts. The first letter identifies the fiber material (C = carbon), the second part of the label indicates the fiber type and condition, Dry and ER, respectively. The final part of the label shows the maximum temperature (°C) level to which the specimens were exposed before testing. Three specimens were tested for each FRCM retrofitted case, while only two served as reference ones due to the loss of one specimen during laboratory activities.

2.2 | Materials and specimens realization

Concrete specimens were cast using the same concrete batch with a mix designed for a low strength class in order to simulate existing under-designed concrete elements that need strengthening. The mix design of the concrete batch was realized with roundish limestone aggregates in two fractions, 0–4 mm and 4–16 mm (45% and 55% respectfully), 300 kg/m^3 of cement CEM 32.5 II/A-LL type, water/cement ratio of 0.6, and 0.2% on cement weight plasticizers agent to improve the workability class. After demolding, all concrete specimens were cured in water at 20 ± 2°C for 28 days, before confining them with carbon FRCM. Retrofitted elements were left curing covered by humid tissues and placed inside plastic bags at 20 ± 2°C. Before high temperature testing, specimens were left curing for a total of at least 90 days since the confining jacket was applied, in accordance with the curing conditions of the RILEM recommendations.[39] The average unconfined compressive strength at the time of testing is $f_{c0} = 20.87$ evaluated on standard 150 × 300 mm ($d \times h$) concrete cylinders.

For the FRCM composite, the reinforcement consists in two types of carbon fabric: one in dry condition and the other impregnated using an ER solution. It should be highlighted that the two carbon fabrics differ also in the equivalent thickness, with the latter being slightly heavier than the former one. The inorganic matrix consists in a premixed fiber-reinforced cementitious mortar with a declared compressive strength at 28 days of 25 MPa. All materials for the FRCM system were provided by the same manufacturer. The properties of the carbon fibers, provided by the manufacturer,[40,41] are shown in Table 1. Different mortar batches were mixed for each confined concrete specimens. Since mortar properties may vary among different mixtures depending on the applied moisture and placing conditions, three prismatic specimens, with 40 × 40 × 160 mm dimensions, were cast during the application of the confining jacket of each cylinder, cured under the same conditions and tested to evaluate the compressive (f_{cm}) and flexural (f_{fm})

TABLE 1 Properties of carbon fabric.

Material	t_f (mm)	E_f (GPa)	f_f (MPa)	ε_f (%)
Carbon	0.047 0.061	240	4900	1.80

strength according to Reference 42. The results are given in Table 2 for each confined specimen. Based on the previous experience of the authors and in order to permit an easy comparison of the results between specimens of the same type, two FRCM layers were used for the confining jacket.

The FRCM confinement jacket was applied after 28 days of curing always following the same protocol that is shown in Figure 1. The concrete specimen was initially damped with water to avoid water absorption from the FRCM composite and promote adherence with the substrate. A first layer of mortar (about 3–4 mm of thickness) was applied around the cylinder and, above it, the carbon fabric was wrapped, gently pushing it into the matrix. Afterwards, a second layer of mortar was applied covering the carbon fabric and the same procedure was repeated for the second carbon fabric layer, which, was covered with a final layer of mortar. Carbon fabric was applied continuously with a final overlapping length of about 200 mm. During the wrapping operations the fabric was maintained under slight tension to avoid bubbles formation and imperfect contact. The overall FRCM jacket thickness was about 10–12 mm. Note that the confining jackets were applied leaving about 10 mm uncovered at the top and bottom of the cylinders, to ensure that the axial load is applied on the concrete core only, in order to avoid direct axial load onto the jacket. After the strengthening procedure, specimens were covered with humid tissues, put in plastic bags, and left to cure.

2.3 | Test set-up and loading protocol

After at least 90 days of curing and before axial compression testing, specimens were subjected to increasing heating–cooling cycles with maximum temperature levels being: 80°C, 100°C, 250°C, while the reference specimens were tested at ambient temperature (i.e., 20°C). Each cycle consists of three phases: heating-up, stabilization at constant temperature, and finally cooling to ambient temperature. The heating cycles were performed in an electric oven and the temperature was monitored by two type K thermocouples, connected to a data acquisition system. The heating rate, estimated from thermocouples records after the heating cycles were performed, results

TABLE 2 Specimens' features.

	Geometry		Fabric properties			Matrix properties		
Specimen	D (mm)	h (mm)	Fabric layers	t_f (mm)	Carbon fabric	f_{cm} (MPa)	f_{fm} (MPa)	T (°C)
C_Dry_20_1	150	300	2	0.047	Dry	26.03	4.54	20
C_Dry_20_2	150	300	2	0.047		28.36	5.01	20
C_Dry_20_3	150	300	2	0.047		29.81	5.04	20
C_Dry_100_1	150	300	2	0.047		27.68	4.61	100
C_Dry_100_2	150	300	2	0.047		29.16	4.83	100
C_Dry_100_3	150	300	2	0.047		25.57	4.20	100
C_Dry_250_1	150	300	2	0.047		33.51	6.57	250
C_Dry_250_2	150	300	2	0.047		33.73	6.26	250
C_Dry_250_3	150	300	2	0.047		31.92	6.25	250
C_ER_20_1	150	300	2	0.061	Epoxy coated	23.84	4.15	20
C_ER_20_2	150	300	2	0.061		19.89	3.99	20
C_ER_20_3	150	300	2	0.061		21.30	4.41	20
C_ER_80_1	150	300	2	0.061		28.53	5.44	80
C_ER_80_2	150	300	2	0.061		23.96	4.72	80
C_ER_80_3	150	300	2	0.061		23.77	4.54	80
C_ER_100_1	150	300	2	0.061		21.57	4.78	100
C_ER_100_2	150	300	2	0.061		19.83	4.59	100
C_ER_100_3	150	300	2	0.061		18.17	4.20	100
C_ER_250_1	150	300	2	0.061		27.96	5.02	250
C_ER_250_2	150	300	2	0.061		27.54	5.80	250
C_ER_250_3	150	300	2	0.061		17.84	3.98	250

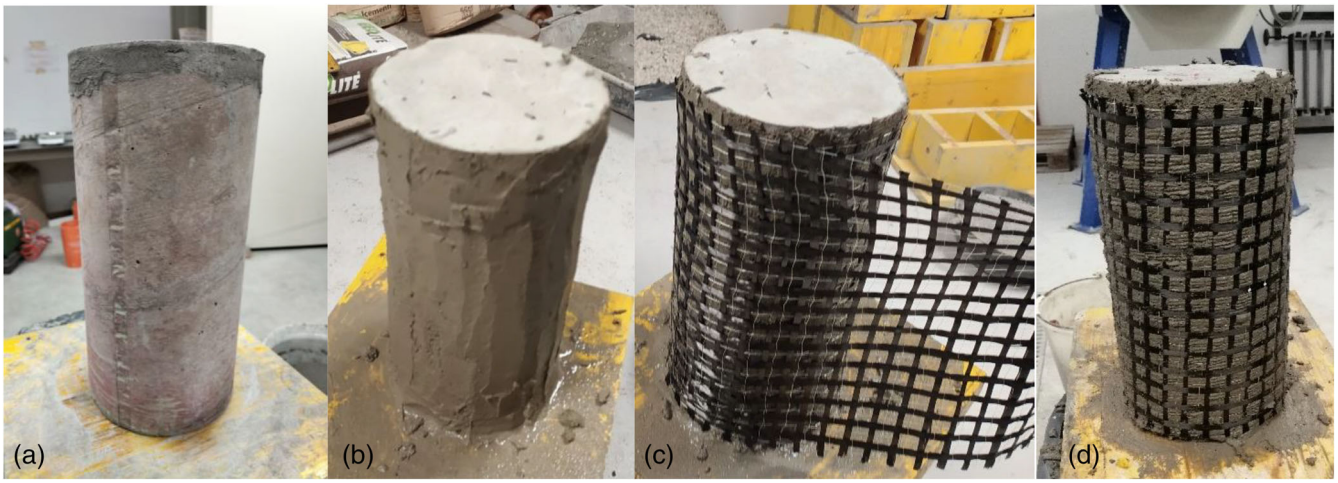

FIGURE 1 FRCM confining jacket application procedure: (a) wet concrete cylinder, (b) first matrix layer application, (c) first fabric wrapping, and (d) complete carbon fabric application. FRCM, fabric-reinforced cementitious matrix.

at about 4°C/min for temperatures up to 100°C, while for higher temperatures the heating rate slows down due to water evaporation and, for specimens confined with coated fabrics, due to polymeric melting. To allow a uniform temperature diffusion on the entire specimens' volume, the stabilization phase was kept for 6 h, similar to what was previously carried out by Reference 36 on thermally conditioned PBO-FRCM-confined cylinders. Only specimens confined with coated carbon fabric were exposed to an additional temperature level of 80°C temperature. This aimed to investigate if the epoxy coating would undergo any degradation even for temperatures lower than 100°C, given the poor behavior of organic matrixes in temperatures above the glass transition temperature (T_g).

After cooling down, specimens were axially loaded adopting a compression cyclic loading protocol. The tests were carried out using a universal loading machine with a 600 kN capacity under displacement control mode. Single compressive cycles were performed using a displacement rate of 0.6 mm/min for both loading and unloading paths. The test was considered complete when a significant reduction of the axial load capacity was observed, generally being lower than 50% of the peak load. To avoid complete unloading and undesired movement of the specimens or of the instrumentations a small axial load of about 0.5 MPa was maintained during the unloading cycles. Before testing, both the top and bottom faces of the cylinder were capped with high-strength mortar to ensure a proper distribution of the axial loading.

The axial load was acquired continuously during the test, using the 600 kN load cell of the universal testing machine. Axial strains were monitored using three linear voltage displacement transducers (LVDTs), which acquired the displacement between the top and bottom plates. LVDTs were installed equally spaced at 120° angle. Figure 2 shows the setup adopted for the testing.

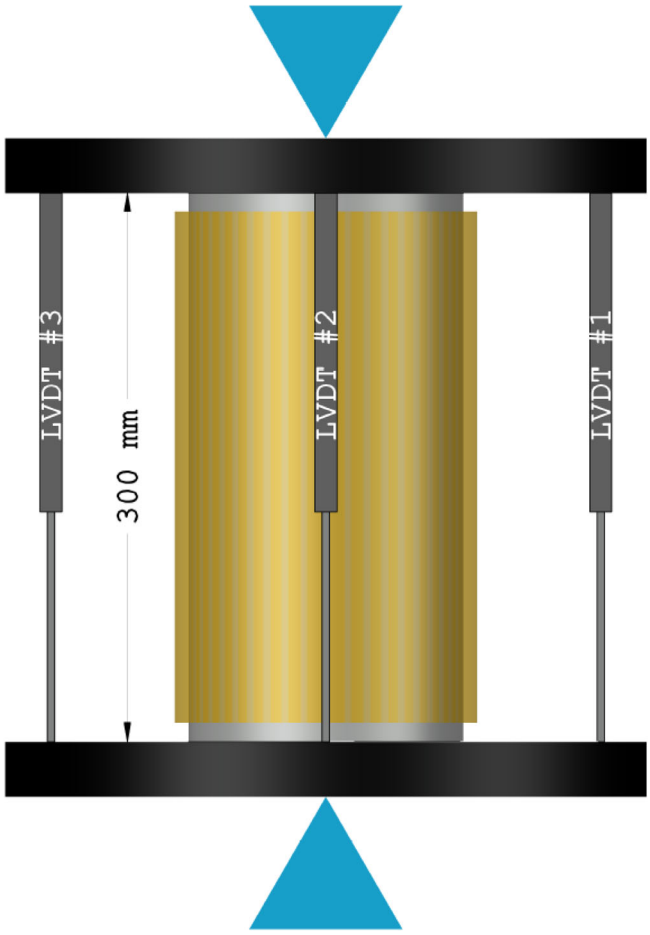

FIGURE 2 Test setup.

3 | RESULTS AND DISCUSSION

Regardless of the materials employed, confinement is one of the main retrofitting techniques used to rehabilitate axially loaded elements. The effects of the external confining jacket are beneficial both in terms of strength gain and axial ductility enhancement, while, if direct axial loading of the confining jacket is avoided, the effect of the confinement system on the axial stiffness can be considered negligible. Previous research has shown that when dealing with FRP[43] or FRCM jackets,[44] depending on the several parameters that affect the confinement effectiveness (i.e., materials, number of layers in the confinement, cross-section shape, initial unconfined strength, etc.), the confined axial stress–strain curve can have a pure softening (curve *a*), initial descending followed by a plateau (curve *b*), or hardening behavior (with or without an initial descending branch, respectively curve c' and c''). The idealized axial stress–strain curves for confined concrete are shown in Figure 3.

In the following paragraphs the axial behavior is discussed in terms of peak axial stress and corresponding strain (f_{c0}, ε_{c0}) for unconfined specimens. For confined ones, depending on the axial stress–strain curve shown during experimental testing, stress and corresponding strain at first peak ($f_{cc,1}$, $\varepsilon_{cc,1}$), confined ultimate axial strength (f_{ccu}), and corresponding ultimate axial strain (ε_{ccu}). Tables 3 and 4 summarize the main experimental results for the unconfined and confined tested specimens, respectively. For specimens with type *b* or c' axial stress–strain curve, the confined axial strength at the first peak $f_{cc,1}$ and strain $\varepsilon_{cc,1}$ are also given in the tables. Other than the above-mentioned main parameters, in Table 4, the strength enhancement with respect to the unconfined peak stress (f_{cc}/f_{c0}) and the ratio between the peak strength for specimens subjected to a maximum temperature T and specimens at ambient temperature (20°C) ($f_{cc,T}/f_{cc,20}$) are reported. When specimens show an initial descending branch in the stress–strain behavior (type *b* and c' curves) the axial strength is assumed as the maximum between stress recorded at first and at ultimate point, $f_{cc} = \max(f_{cc,1}; f_{ccu})$. Lastly, as an axial ductility index, the ratio of the axial strain at failure (ε_{ccu}) over the axial strain at peak load for unconfined specimens (ε_{c0}) is given in the last column of Table 4 ($\varepsilon_{ccu}/\varepsilon_{c0}$).

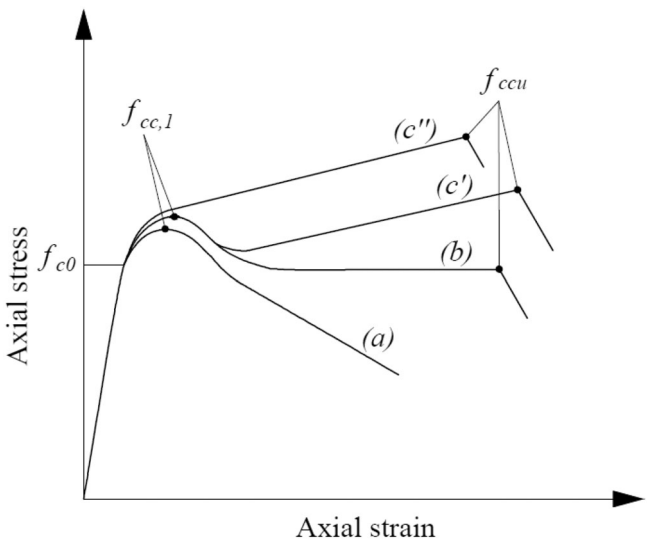

FIGURE 3 Axial stress–strain behavior (envelope) and definition of the ultimate conditions for (a) unconfined concrete and (b) FRCM-confined concrete.[44] FRCM, fabric-reinforced cementitious matrix.

3.1 | Axial stress–strain behavior

Unconfined and confined specimens were cast using the same concrete batch, therefore, the initial concrete strength (f_{c0}) is the same for all considered cases. Stress–strain curves for all the tested specimens are shown in Figure 4. It can be observed that similar axial stress–strain behavior between specimens of the same type and under the same conditions were recorded, showing consistency and reliability of the experimental results.

The unconfined compressive strength was obtained on two $d \times h = 150 \times 300$ mm reference cylinder specimens and the results showed a mean compressive strength of 20.87 MPa while the axial strain at peak stress was about 0.34%. At ambient temperature, specimens confined with dry carbon fabric exhibited a similar axial behavior to what is idealized by curve *b* and c' in Figure 3. After the first peak strength, which was reached at almost the same axial strains of unconfined specimens, in one case over three a slight decrease in the load bearing capacity was observed, then followed by an almost constant load until failure. Instead, in the other two cases, a slight strength gain in the post-peak branch was observed. A similar behavior was observed also for two of the three specimens confined with dry carbon fabric and heated up to 100°C, while one specimen showed a clear hardening behavior without an initial strength loss (curve c''). This type of stress–strain behavior is in line with some previous results obtained on concrete specimens confined through dry carbon fabric FRCM jacket.[9]

TABLE 3 Results of unconfined specimens.

Specimen ID	f_{c0} (MPa)		ε_{c0} (−)	
NC1	19.95	20.87	0.0032	0.0034
NC2	21.91		0.0036	

TABLE 4 Results of confined specimens.

Specimen	$f_{cc,1}$ (MPa)	$\varepsilon_{cc,1}$ (%)	f_{ccu} (MPa)	ε_{ccu} (%)	Curve type	f_{cc}/f_{c0}	$f_{cc,T}/f_{cc,20}$	$\varepsilon_{ccu}/\varepsilon_{c0}$
C_Dry_20_1	26.78	0.0037	26.31	0.0085	*b*	1.28	1.00	2.50
C_Dry_20_2	25.44	0.0033	24.76	0.0084	*b*	1.22		2.47
C_Dry_20_3	24.97	0.0035	23.80	0.0078	*b*	1.20		2.29
C_Dry_100_1	–	–	23.81	0.0090	c''	1.14	0.93	2.85
C_Dry_100_2	20.37	0.0035	20.82	0.0095	c'	1.00	0.81	2.88
C_Dry_100_3	21.89	0.0040	21.02	0.0096	c'	1.05	0.85	2.82
C_Dry_250_1	–	–	21.58	0. 0071	c''	1.03	0.84	2.35
C_Dry_250_2	–	–	21.18	0.0070	c''	1.06	0.86	2.21
C_Dry_250_3	–	–	21.61	0.0083	c''	1.04	0.84	2.62
C_ER_20_1	–	–	30.40	0.0146	c''	1.50	1.00	4.53
C_ER_20_2	–	–	27.32	0.0115	c'	1.31		3.88
C_ER_20_3	–	–	29.48	0.0085	c''	1.41		2.82
C_ER_80_1	–	–	30.37	0.0115	c''	1.46	1.03	3.56
C_ER_80_2	–	–	29.13	0.0113	c''	1.40	0.99	3.62
C_ER_80_3	–	–	28.66	0.0107	c''	1.37	0.97	3.62
C_ER_100_1	–	–	28.24	0.0138	c''	1.35	0.96	4.41
C_ER_100_2	–	–	29.78	0.0158	c''	1.43	1.01	4.65
C_ER_100_3	–	–	29.40	0.0131	c''	1.41	1.00	4.47
C_ER_250_1	–	–	27.56	0.0123	c''	1.32	0.94	3.62
C_ER_250_2	–	–	26.10	0.0146	c''	1.25	0.89	4.47
C_ER_250_3	–	–	26.73	0.0120	c''	1.28	0.91	4.59

However, when concrete cylinders confined with dry carbon FRCM are exposed to a temperature of 250°C, the axial behavior changes definitively from that of a curve *b* or c' to that described by curve c'', showing a pure hardening behavior. This change should not be associated with an overall better performance of the specimens at high temperature as it is just a change of curve shape due to a reduction of confined strength at low axial strains. Note that both the peak strength and strain are reduced compared to the case of specimens tested without a thermal conditioning.

Specimens confined with epoxy-coated carbon fabric exhibited all the same type of axial behavior, that is described by curve c'' of Figure 3. At ambient temperature, some differences are observed between the three tested specimens: one had the best performance, with a clear hardening behavior up to axial strain values of about 1.5%. In specimens 2, the hardening branch is marked by only a very slight slope, however exhibiting a good axial ductility. Lastly, the third specimen followed the same trend as C_ER_20_1, but the failure was observed slightly before 1% of axial strain was reached. At increasing temperatures, the differences among the axial stress–strain curves of the three tested specimens of the same type are minimal.

3.2 | Effect of temperature exposure

3.2.1 | Dry carbon FRCM

For the sake of comparison, envelope curves of the cyclic stress–strain behavior are plotted in Figure 5 for dry and epoxy-coated carbon fabric, respectively a) and b). At ambient conditions, concrete cylinders confined with dry carbon FRCM show a significant strength gain at the first peak and then, after some amount of load bearing capacity loss, the strength is maintained almost constant, or a new slight strength gain is recorded, up to axial strains above 0.8%. When the same confined elements are exposed to high temperatures, the gain at the first peak (occurring at low strain values) is lost. At axial strain values close to ε_{c0}, stress values similar to the unconfined concrete strength f_{c0} are recorded. After this point, a hardening branch follows, which still provides a good axial ductility despite the high temperature exposure. Compared to the unconfined specimens, confined ones have always a better performance even after exposure at 100 and 250°C, with about 6% and 4% strength gain on average. However, when compared to the confined strength at ambient temperature, a reduction of about 15% is observed for both temperature levels. For

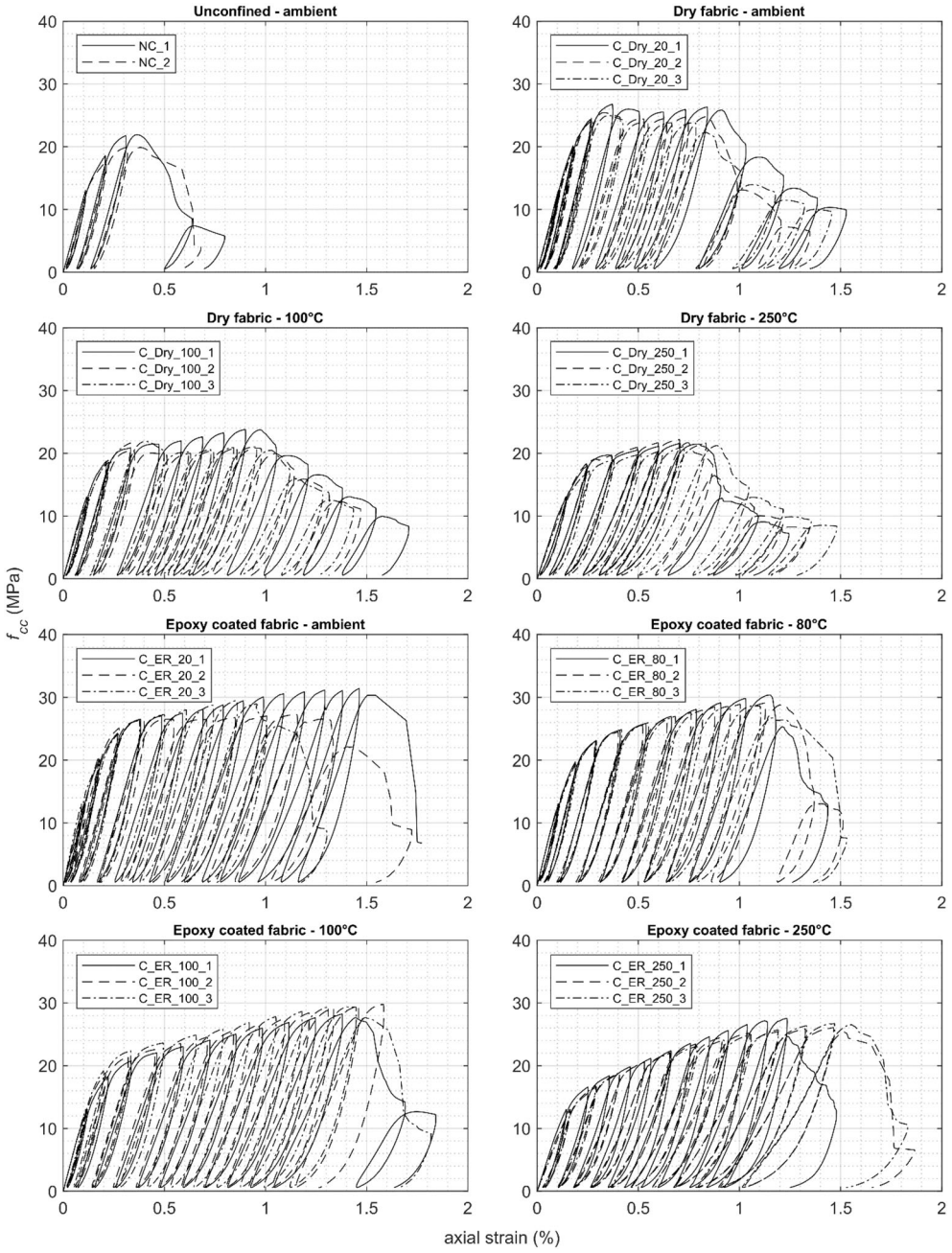

FIGURE 4 Axial stress–strain behavior of the tested specimens.

specimens confined with dry carbon FRCM, no significant differences were observed between specimens exposed at 100 and 250°C, apart from a slight decrease in the initial stiffness. In fact, concrete is typically characterized by a decrease of the elastic properties in this range of temperature.[45,46]

3.2.2 | Coated carbon FRCM

Cylinders confined with epoxy-coated carbon FRCM, at axial strains close to ε_{c0}, showed a similar strength gain to those confined with dry fabric when not subjected to heating. However, when increasing the exposure temperature, a gradual loss of this strength gain was observed. In fact, for 100°C temperature, axial stress values at ε_{c0} are close to the unconfined concrete strength, while for cases exposed to 80 and 250°C stress values result slightly higher and lower, respectively. Almost all specimens show a clear hardening behavior, reaching the failure at particularly high axial strains. Independently of the clear change in the axial behavior at low strain values, in terms of overall strength, specimens confined with epoxy-coated carbon maintain almost the same effectiveness: on average, the strength enhancement is about 40% compared to the initial unconfined strength, even when

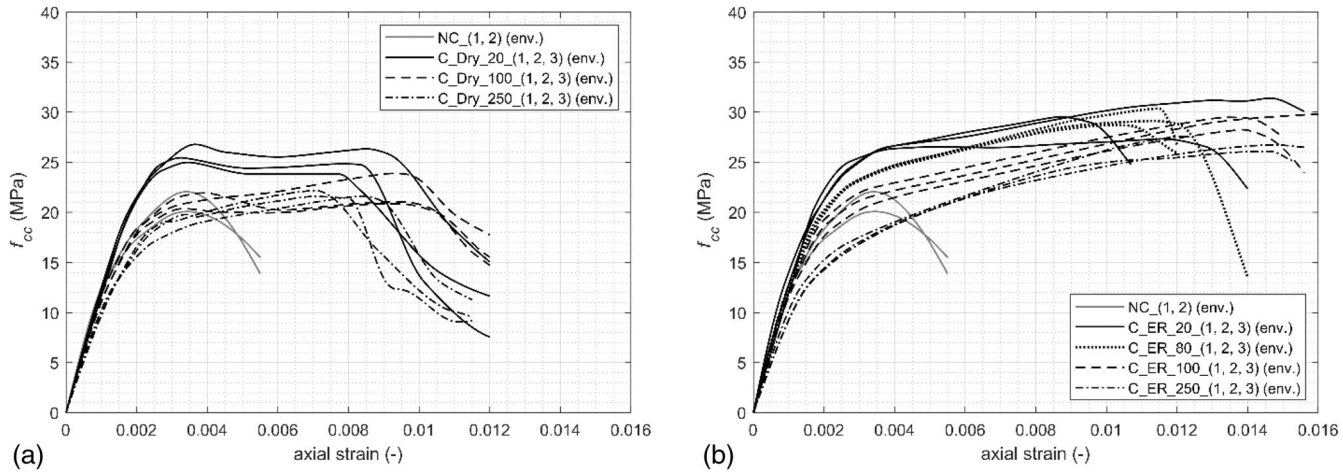

FIGURE 5 Comparison between axial stress–strain curves for different temperatures for dry (a) and epoxy-coated (b) carbon fabric.

exposed to 80 and 100°C. After exposure to 250°C, the confined compressive strength results still higher than the initial unconfined one, maintaining a strength gain of about 28%. The axial ductility results similar as well, among all specimens, with a slight increase in the axial strain capacity for specimens exposed to high temperatures. Melting of the coating during heating and re-stiffening after cooling down is believed to be the reason for the good performance in terms of residual strength for epoxy-coated FRCM jackets. This behavior agrees with previous observation in literature, for example, de Andrade Silva et al.[31] observed an improvement in the fiber-matrix bond for coated yarns in pull-out tests for temperatures levels below 200°C. According to this study, when reaching the glass transition temperature of the coating, its mechanical behavior transforms from visco-elastic to plastic and the volume expansion pushes it into the small pores of the surrounding cementitious matrix. When cooling down to room temperature, the coating becomes stiffer and visco-elastic again, but a complete retraction of copolymer from the matrix pores is not possible due to the adhesive forces between the polymer and the hydration product surfaces in the matrix. This mechanism of matrix–polymer interlocking enhances the bond between the fabric and the matrix, and consequently permits to maintain high confining strength even after exposure to some level of high temperature. However, this kind of favorable behavior is lost when the temperature level starts to affect the polymer structure and to cause its decomposition. Pull-out tests at 400°C showed that fiber-matrix bond of coated fibers can result significantly worst with respect to dry ones.[31] It should be also highlighted that the melting of the coating during high temperature exposure may significantly affect the composite strength and the retrofitting effectiveness at the hot-state. Further evidence should be collected from new experimental tests to confirm this behavior under cyclic axial solicitation.

3.2.3 | Dry versus epoxy-coated carbon FRCM jacket

Figure 6 shows the envelope axial stress–strain curves for specimens confined with dry and epoxy-coated carbon fabric for each temperature exposure level. Instead, Figure 7 summarizes the values assumed by two ratios: first (a), the ratio between the residual confined strength after temperature exposure and the unconfined strength ($f_{cc,T}/f_{c0}$); then (b), the ratio between the residual confined strength after temperature exposure and the confined strength at ambient temperature ($f_{cc,T}/f_{cc,20}$). Results are reported both for dry and coated carbon FRCM jackets.

The behavior of the confined specimens with dry and coated fabrics remains very similar in the first stage of the axial stress–strain curves for all temperature levels, while the difference becomes more significant in the last stage, that is, for high axial strain values.

In terms of compressive strength, even though, due to the difference in fabric thickness, the results cannot be directly compared in a quantitative way, Figure 7 allows for a qualitative comparison between specimens confined with dry and coated fabrics. A similar trend can be observed in both Figure 7a,b. Specimens with coated fabric maintain an almost unaltered residual strength up to 100°C. After that, a slight reduction is observed at 250°C exposure. On the other hand, specimens with dry carbon fabric show immediately a significant decrease in confined compressive strength already at 100°C temperature exposure. However, the residual strength does not decrease with the increase of thermal stress, maintaining an almost constant value, at least until the maximum investigated temperature (i.e., 250°C). The authors believe this occurs because specimens confined with dry carbon fabric show a type *b* or *c′* curve in their axial stress–strain behavior and the maximum strength is generally observed at the first peak ($f_{cc,1}$ in Figure 3).

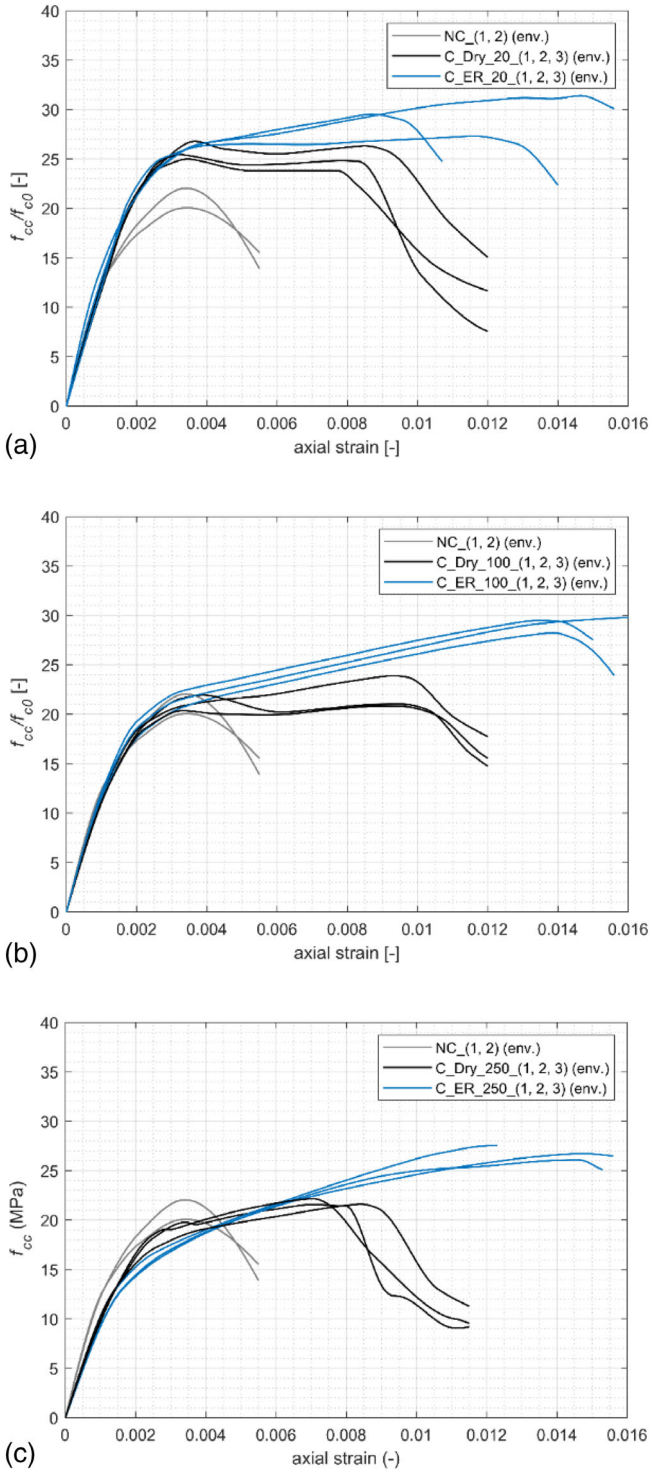

FIGURE 6 Envelope axial stress–strain curves for dry and epoxy-coated carbon FRCM at (a) ambient temperature, (b) 100°C, and (c) 250°C.

According to Reference 44, the gain at this point is mainly due to the overall matrix-fabric stiffness, as lateral strains in the concrete sample are still very low to fully activate the composite reinforcement and cracks propagation in the matrix is still limited. Loss of strength gain at this point was observed for all specimens subjected to high temperatures and is believed to be due to the cracking of the FRCM matrix after temperature exposure (Figure 8). With the matrix already cracked the initial stiffness of the confining system is reduced and therefore the confinement effectiveness at low strain levels also. For specimens exposed to 250°C, that show all a type c'' axial stress–strain curve, the slope of the hardening branch results to be the highest for those confined with coated carbon fabric, highlighting higher axial stiffness and better overall performance compared to the dry ones. The initial matrix cracking does not have a significant influence on the confinement performance after high axial strains are reached as at this point the matrix results fully cracked due to the lateral expansion of the axially loaded concrete specimen.

To compare epoxy and dry specimens directly and mitigate the effect of different fabric thicknesses the ratio between the gain in compressive strength with respect to the initial unconfined strength ($f_{cc,T} - f_{c0}$) and the lateral confining pressure exerted by the FRCM jacket (f_l) is computed and is shown in Figure 9. The confining pressure is calculated as:

$$f_l = \frac{2 \cdot n_f \cdot t_f \cdot E_f \cdot \varepsilon_{fu}}{D} \quad (1)$$

The calculated ratio indicates the strength gain (in MPa) for unit lateral pressure provided by the jacket. It is clear that the epoxy coating enhances the performance of the composite at all considered temperature levels. At ambient temperature, the performance of the jackets, per unit of lateral pressure, differs by approximately 30%, corresponding almost to the difference in reinforcement amount present in the composites. The difference is more market after temperature exposure, where the contribution of 1 MPa of confining lateral pressure to the gain in compressive strength is more than four times higher for specimens that embed coated carbon fabric.

3.3 | Failure modes

Among specimens confined with the same type of carbon fabric, no significant differences were observed in the failure modes of specimens exposed to different temperature levels (Figure 10). Generally, specimens displayed a homogeneous and uniform vertical crack pattern and larger cracks were concentrated in the upper part of the FRCM jackets. After the ultimate load is reached, very few new crack openings were observed in all specimens. In cylinders confined with dry carbon FRCM, failure was reached with the continuous propagation of one or few of the existing main cracks that developed. The main failure crack is generally close to the overlapping start or end of the fabric layer, highlighting the failure due to fiber

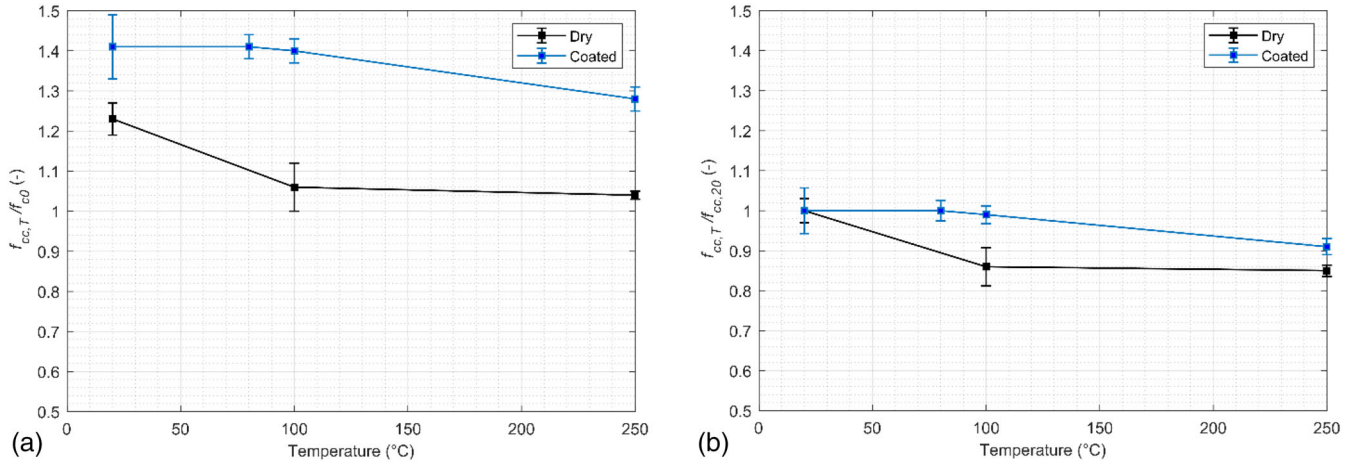

FIGURE 7 Ratio between (a) confined and unconfined strength ($f_{cc,T}/f_{c0}$) and (b) confined strength after temperature exposure and confined strength at ambient temperature ($f_{cc,T}/f_{cc,20}$).

FIGURE 8 Matrix cracking after high temperature exposure.

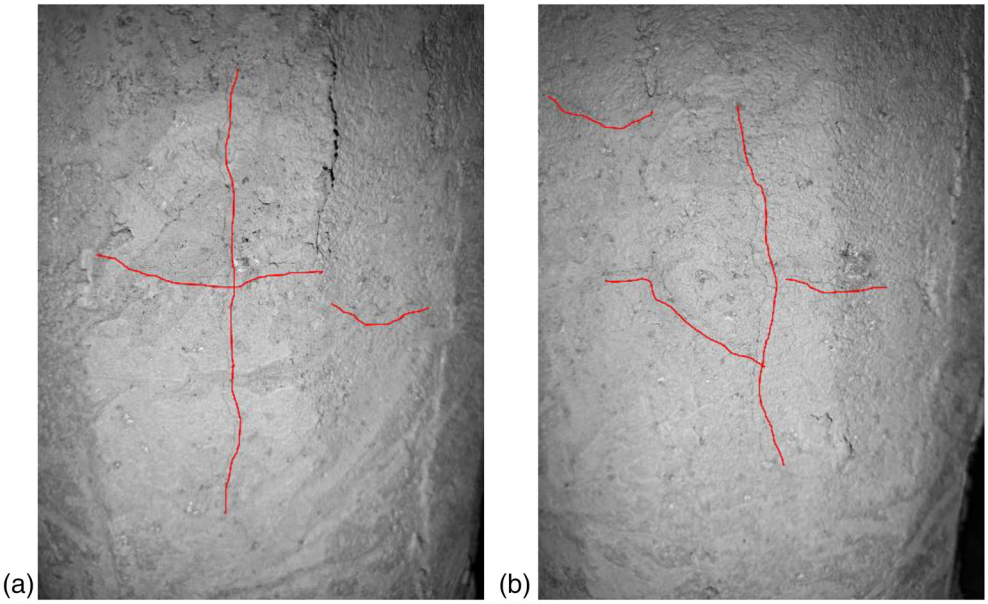

slippage in the matrix. In specimens confined with epoxy-coated FRCM, failure was more abrupt and was reached by a clear delamination in the overlapping zone. In this case fiber rupture was clearly observed, while in specimens with dry fabric only partial fiber rupture was observed in the external part of the yarns, due to a telescopic failure. For specimens confined with ER-impregnated fibers, the spalling of the external mortar layer was observed similarly in Reference 10.

3.4 | Theoretical confined strength prediction

Different confinement models are available in literature and can be used to predict the strength enhancement for concrete confined through FRCM composites. Commonly, they are calibrated on confined specimens having different cross-section shapes, confining layers, fiber materials, initial unconfined concrete strength, etc. However, there are no models based on specimens subjected to high temperatures. In the range of temperatures investigated in the present study the results shows that the main effect of the high temperatures is concentrated in the first peak on the stress strain curve (i.e., at low axial strains), while the ultimate point, is little affected. Hence, at least for temperatures up to 250°C, models that do not specifically account for temperature exposure could still provide a relatively good prediction for the experimental results. In this section, the experimental results obtained during the experimental campaign are compared to the theoretical ones obtained applying six existing FRCM-confined concrete models from literature, namely those proposed by the Italian CNR guidelines,[47]

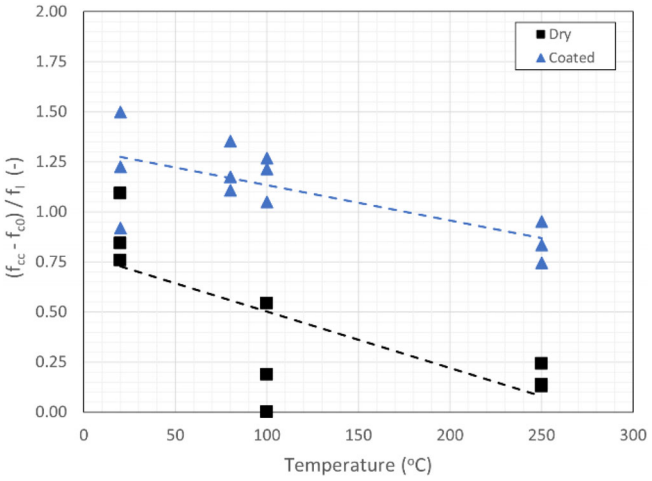

FIGURE 9 Ratio between the gained compressive strength ($f_{cc} - f_{c0}$) and the lateral pressure (f_l) of the confining FRCM jacket. FRCM, fabric-reinforced cementitious matrix.

ACI549.4R guidelines,[48] Triantafillou et al.,[49] Ombres and Mazzuca,[50] Cascardi et al.,[51] and Toska and Faleschini.[44] All formulations consider two main parameters, the initial unconfined strength and the lateral confining pressure. They all come from the mathematical equation proposed by Richart et al.,[52] and none consider the effect of the high temperature exposure. Instead, the proposals differ mainly on the equation coefficients, calibrated on different dataset of experimental results, and on the reduction factors of fiber strain limitations introduced to calculate the effective lateral pressure.

The ACI549.4R formulation is given through a linear equation, while all the other models use a nonlinear form. Only CNR-DT 215,[47] Cascardi et al.,[51] and Toska and Faleschini[44] formulations take into account the matrix properties in their formulations, although through different ways. CNR-DT 15[47] and ACI549.4R[48] equations limit directly the maximum fiber strain (with the former being much more restrictive), while Ombres and Mazzuca[50] approach accounts for fiber strain limitation through an effectiveness coefficient k_e, that is computed based on the axial stiffness of the confining jacket ($\rho_f E_f$) and the initial unconfined strength of concrete (f_{c0}). Finally, the confinement model proposed recently by Toska and Faleschini distinguishes between the different axial stress–strain behaviors that can be observed on FRCM-confined concrete and proposes two formulations to predict the confined strength at the first peak ($f_{cc,1}$) and the confined strength at the ultimate point (f_{ccu}). In this case, based on the stress–strain curve exhibited by the specimens (Figure 3), the respective formulation can be used to compute the peak strength.

The experimental confined strength for the tested specimens is compared with the theoretical one predicted using the existing models shown in Table 5, and the results are summarized in Table 6 in terms of $f_{cc,theo}/f_{cc,theo}$ ratio and in Figure 11 as experimental versus predicted confined compressive strengths ($f_{cc,exp}$ vs. $f_{cc,theo}$) plots. In addition, some statistical parameters as: mean $f_{cc,theo}/f_{cc,theo}$ value, mean absolute error (MAE), and root mean squared error (RMSE), are computed.

Results show that all considered models, except from Reference 44, perform poorly in the prediction of the confined strength of FRCM-confined concrete exposed to high temperatures. The ACI54.4R-20[48] appears to be the most unconservative model with a mean $f_{cc,theo}/f_{cc,exp}$ value about 1.3, followed by Cascardi et al.[42] that overestimates the confined compressive strength by about 12%. In terms of mean $f_{cc,theo}/f_{cc,exp}$ values, the formulation proposed by CNR-DT 215[47] and Triantafillou et al.[49] shows a more conservative behavior, respectively, 92% and 94%. Cascardi et al.[51] estimates quite well the confined strength of specimens not subjected at high temperatures, but it overestimates significantly the results for cylinders confined with dry carbon FRCM subjected to high temperatures. In terms of mean error, again, ACI549.4R-20 shows the worst results with a mean error of about 30%. Other models' mean error ranges between 10% and 14% while the one proposed by Toska and Faleschini shows a very limited error (about 5%). The poor performance of the existing models for specimens subjected to high temperature is somehow expected, as none of these formulations consider a parameter to account for the damage induced by the high temperature.

However, mean $f_{cc,theo}/f_{cc,exp}$ values do not express adequately the models' performance as, sometimes, underestimations and overestimations are compensated resulting in a mean value close to the unit. For this reason, the overall performance of the existing models is better shown by Figure 11. Most of the existing models show a constant trend in their prediction (i.e., horizontal alignment of the points in Figure 11). This means that the considered parameters are not enough to model the variability of the results. Models that do not account for the matrix properties in their formulations predict the confinement strength only based on the fabric properties and the results' variation is only based on the fabric thickness used in the FRCM jackets. This is shown by two distinct lines created by the results of ACI549.4R-20, Triantafillou et al., and Ombres and Mazzuca in Figure 11. The possible introduction of a reduction factor to consider the temperature effect may be effective to improve the prediction, even if it appears clear that most of the variability that characterizes the experimental results cannot be predicted unless a proper calibration is performed on a wide dataset. Models that consider matrix properties are much more accurate to reproduce the variability of the results, even in absence of a temperature-correlated coefficient. However, this influence is little observed in

FIGURE 10 Failure modes: (a) NC, (b) C_Dry_20, (c) C_Dry_100, (d) C_Dry_250, (e) C_ER_20, (f) C_ER_80, (g) C_ER_100, and (h) C_ER_250.

the CNR-DT 215 results, which estimates very similar compressive strength values for all considered cases. Cascardi et al. seems to predict quite well the experimental results of specimens not subjected to high temperatures (plotted points aligned with the ideal diagonal) while the model proposed by Toska and Faleschini performs best,

TABLE 5 Existing FRCM confinement models.

Source	Model	Notes
CNR-DT 215[47]	$\frac{f_{cc}}{f_{c0}} = 1 + 2.6\left(\frac{f_{l,eff}}{f_{c0}}\right)^{\frac{2}{3}}$	$f_{l,eff} = k_h \cdot f_l$ $k_h = 1 - \frac{(b-2r_c)^2+(h-2r_c)^2}{3bh}$ $f_l = \frac{2 \cdot n_f \cdot t_f \cdot E_f \cdot \varepsilon_{fu,rid}}{D}$ $\varepsilon_{fu,rid} = min\left(\eta_A \cdot k_{mat} \cdot \frac{\varepsilon_f}{\gamma_m}; 0.004\right)$ η_A is the environmental coefficient γ_m is the safety partial coefficient (1.5) $k_{mat} = 0.217\left(\rho_{mat} \cdot \frac{f_m}{f_{c0}}\right)^{3/2} \leq 1$ $\rho_{mat} = \frac{4 \cdot t_m}{D}$
ACI549.4R[48]	$f_{cc} = f_{c0} \cdot \left(1 + 3.10 \cdot k_a \cdot \frac{f_l}{f_{c0}}\right)$	$k_a = \frac{A_e}{A_c}\left(\frac{b}{h}\right)^2$ $\frac{A_e}{A_c} = \left[1 - \frac{\frac{h}{b}(b-2r_c)^2+\frac{b}{h}(h-2r_c)^2}{3bh}\right]$ $f_l = \frac{\rho_f \cdot E_f \cdot \varepsilon_{fe}}{D}$ $\varepsilon_{fe} = \varepsilon_f \leq 0.012$
Triantafillou et al.[49]	$f_{cc} = f_{c0} \cdot \left[1 + 1.9 \cdot \left(\frac{f_{l,eff}}{f_{c0}}\right)^{1.27}\right]$	$f_{l,eff} = k_e \cdot \frac{(b+h)}{bh} \cdot t_f \cdot E_f \cdot \varepsilon_f$ $\frac{b+h}{bh} = \frac{1}{D}$ for circular cross sections $k_e = 1 - \frac{(b-2r_c)^2+(h-2r_c)^2}{3bh}$
Ombres and Mazzuca[50]	$\frac{f_{cc}}{f_{c0}} = 1 + 0.913\left(\frac{f_{l,eff}}{f_{c0}}\right)^{0.5}$	$f_{l,eff} = \frac{1}{2} k_e \rho_f E_f \varepsilon_f$ $k_e = 0.25\left[\left(\frac{\rho_f E_f}{f_{c0}}\right)^{0.3} - 1\right]$
Cascardi et al.[51]	$f_{cc} = f_{c0} \cdot \left[1 + k \cdot \left(\frac{f_l}{f_{c0}}\right)^{2/3}\right]$	$f_l = \frac{n_f \cdot t_f \cdot E_f \cdot \varepsilon_f}{D}$ $k = \frac{4 \cdot \rho_{mat} \cdot f_m}{f_{c0}}$ $\rho_{mat} = \frac{4 \cdot t_m}{D}$
Toska and Faleschini[44]	$f_{ccu} = f_{c0} \cdot \left(0.6 + 1.8 \cdot \left(\frac{f_{l,eff}}{f_{c0}}\right)^{0.55}\right)$ $f_{cc,1} = f_{c0} \cdot \left(1 + \frac{1}{8} \cdot \left(\frac{K_{f,eff}}{f_{c0}}\right)^{\frac{1}{3}}\right)$	$f_{l,eff} = k_h k_m k_f k_t f_l$ $f_l = \frac{2 n_f t_f E_f \varepsilon_f}{D}$ $k_h = 1 - \frac{(b-2r_c)^2+(h-2r_c)^2}{3bh}$ $k_m = \frac{2(n_f+1) f_m}{D}$ $k_f = \begin{cases} 0.3 \text{ carbon, glass and basalt} \\ 0.75 \text{ PBO, epoxy-coated carbon, steel} \end{cases}$ $k_t = 1 - t_f$ $K_{f,eff} = k_h k_m k_f K_f$ $K_f = \frac{2 n_f t_f E_f}{D}$

Abbreviation: FRCM, fabric-reinforced cementitious matrix.

with the $f_{cc,exp}$ versus $f_{cc,theo}$ points well distributed along the diagonal. This is mainly due to the possibility to compute the confined compressive strength at the first peak or at the ultimate point based on the observed behavior. The good performance is also proved in terms of statistical parameters, with a mean $\left(f_{cc,theo}/f_{cc,exp}\right) \cong 1$, MAE = 1.26 MPa, RMSE = 1.70 MPa. The main error observed from the considered models seems to be mainly due to the lack of parameters distinguishing between coated and uncoated fibers, non-consideration of the matrix property, and not accounting for the axial strains where peak load is recorded.

3.5 | Cyclic unloading–reloading path parameters

In this section, the parameters that define the unloading and reloading path during the cyclic loading, being: plastic strains, stress deterioration, and stiffness deterioration for the envelope compression cycles, are presented. All the above parameters are directly related to the envelope unloading strain (ε_{un}).

Plastic strains were not directly recorded during the tests since during the cyclic compressive loading carried out, the unloading path was stopped at an

TABLE 6 Theoretical prediction to experimental result ratio for confined compressive strength ($f_{cc,theo}/f_{cc,exp}$) for the considered confinement models.

	$f_{cc,theo}/f_{cc,exp}$					
Specimen	**CNR-DT 215**[47]	**ACI549.4R-20**[48]	**Triantafillou et al.**[49]	**Ombres and Mazzuca**[50]	**Cascardi et al.**[51]	**Toska and Faleschini**[44]
C_Dry_20_1	0.883	1.197	0.890	1.018	1.058	0.940
C_Dry_20_2	0.940	1.260	0.937	1.072	1.140	0.995
C_Dry_20_3	0.963	1.284	0.954	1.092	1.178	1.016
C_Dry_100_1	1.001	1.346	1.001	1.145	1.210	0.925
C_Dry_100_2	1.152	1.540	1.145	1.310	1.404	1.071
C_Dry_100_3	1.078	1.465	1.089	1.246	1.289	0.988
C_Dry_250_1	1.133	1.486	1.104	1.264	1.413	1.069
C_Dry_250_2	1.104	1.445	1.075	1.230	1.377	1.042
C_Dry_250_3	1.124	1.484	1.103	1.262	1.390	1.055
C_ER_20_1	0.761	1.127	0.796	0.911	0.924	0.927
C_ER_20_2	0.857	1.295	0.915	1.048	1.012	1.008
C_ER_20_3	0.800	1.201	0.848	0.971	0.955	0.953
C_ER_80_1	0.807	1.165	0.823	0.942	1.008	1.015
C_ER_80_2	0.821	1.215	0.858	0.982	0.997	1.001
C_ER_80_3	0.834	1.235	0.872	0.999	1.011	1.015
C_ER_100_1	0.836	1.253	0.885	1.013	1.000	0.999
C_ER_100_2	0.786	1.188	0.839	0.961	0.928	0.924
C_ER_100_3	0.788	1.204	0.850	0.973	0.921	0.912
C_ER_250_1	0.886	1.284	0.907	1.038	1.104	1.111
C_ER_250_2	0.934	1.356	0.958	1.096	1.160	1.168
C_ER_250_3	0.866	1.324	0.935	1.071	1.009	0.997
Mean	0.922	1.303	0.942	1.078	1.119	1.006
Mean error (%)	13%	30%	11%	10%	14%	5%

axial stress of about 0.5–0.6 MPa, in order to avoid undesired movements of the sample or of the measuring instrumentations. Lam and Teng[53] proposed a method for FRP-confined concrete to estimate plastic strains from recorded stress–strain curves with not fully unloaded cycles, by extending the unloading branch to the zero-stress point. The method was previously adopted and used for FRCM-confined concrete by Reference 54.

According to Reference 54, plastic strains can be simply estimated as:

$$\varepsilon_{pl} = \varepsilon_{re} - \frac{f_{re}}{E_{un,0}} \tag{2}$$

where $E_{un,0}$ is the slope of the unloading path to zero, that can be estimated as:

$$E_{un,0} = \min \begin{cases} \dfrac{0.5 \cdot f_{c0}}{\varepsilon_{un}} \\ \dfrac{f_{un}}{\varepsilon_{un} - \varepsilon_{pl}} \end{cases} \tag{3}$$

Generally, $E_{un,0}$ takes the value of the first term in Equation (2) ($0.5f_{c0}/\varepsilon_{un}$), while it can be considered equal to $f_{un}/(\varepsilon_{un} - \varepsilon_{pl})$ when unloading is carried out from very small axial strains.

Stress deterioration during unloading–reloading cycles is considered the ratio between the axial stress corresponding to the unloading strain (ε_{un},f_{un}), just before unloading starts, and the new stress reached during the reloading branch at the previous unloading strain (ε_{un},f_{new}). The new reloading stress (f_{new}) is lower than the unloading one (f_{un}) from the envelope curve, due to stress deterioration occurring after cyclic action in the

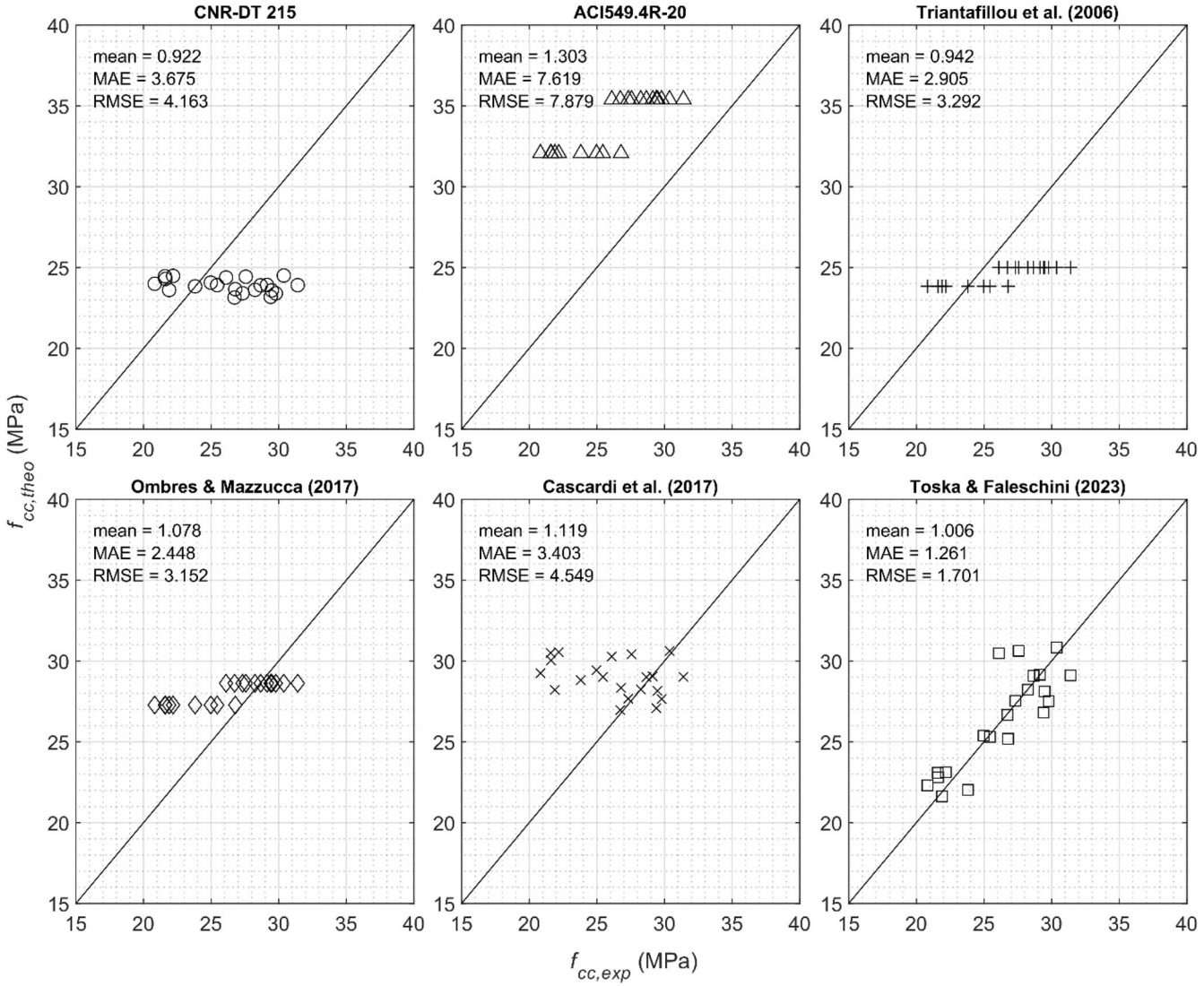

FIGURE 11 Confined compressive strength experimental result versus theoretical prediction for the existing confinement models.

post-peak branch. To describe this phenomenon, a stress deterioration ratio β is defined following a general expression given by:

$$\beta = \frac{f_{\text{new}}}{f_{\text{un}}}, \tag{4}$$

where f_{un} is the envelope unloading stress and f_{new} is the new stress in the reloading path corresponding to the initial unloading strain from the envelope curve. More details and graphical explanation on the parameters can be found in Reference 10.

The initial stiffness of concrete is also affected by the axial cyclic loading. While the unloading path tends to behave linearly at the beginning and then become significantly nonlinear close to the zero-stress zone, the reloading path is generally linear until reaching the unloading strain ε_{un} (at a lower stress value, f_{new}, with respect to the envelope one) and then follows a nonlinear parabolic curve.

The first linear part of the reloading path can be defined by the reloading slope E_{re} that can be computed following Equation (5):

$$E_{\text{re}} = \frac{f_{\text{new}} - f_{\text{re}}}{\varepsilon_{\text{un}} - \varepsilon_{\text{re}}}. \tag{5}$$

The stiffness deterioration, on the other end, is calculated as the ratio of the reloading slope at a certain i cycle ($E_{\text{re},i}$) over the slope at the first cycle $E_{\text{re},0}$.

The results in terms of plastic strains (ε_{pl}), stress deterioration (β), and stiffness deterioration ($E_{\text{re},i}/E_{\text{re},0}$) are plotted versus the unloading strains (ε_{un}) in Figure 12, respectively (a–c). Specimens confined with dry carbon FRCM are plotted in gray, while those confined with

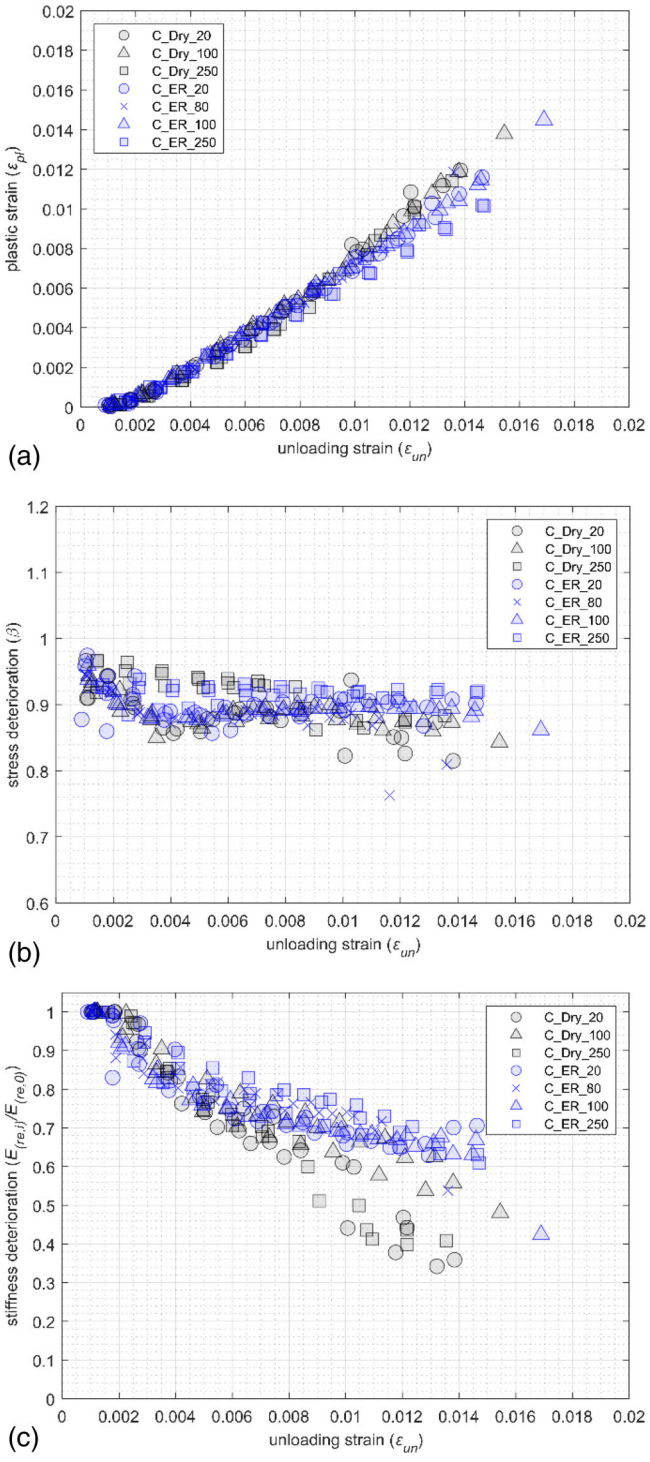

FIGURE 12 (a) Plastic strains, (b) stress deterioration, and (c) stiffness deterioration for dry (gray) and epoxy-coated (blue) carbon FRCM confinement. FRCM, fabric-reinforced cementitious matrix.

epoxy-coated FRCM are plotted in blue. Maximum temperature exposure is distinguished through different marker shapes.

In terms of plastic strains, no significant differences are observed between dry and coated FRCM, independently of the temperature exposure. The slight difference observed for high unloading strain values is due to the fact that specimens confined with dry carbon fabric failed earlier, at axial strains just below 1%.

Regarding stress deterioration (β) a slight effect of high temperature exposure seems to be observed for specimens exposed to 250°C, both with dry and epoxy-coated fabrics. Generally, at very low unloading strains, stress deterioration is very small. As unloading strains increase, β value decreases almost rapidly and then stabilizes at values between 0.9 and 0.85. Similar results were observed in previous experimental works by References 9,10,54. However, for specimens exposed to 250°C, stress deterioration was more gradual and did not show the rapid decrease generally observed for unloading strains between 0.002 and 0.004.

No significant differences were observed for stiffness deterioration too. Deterioration results similar for both dry and epoxy-coated cases until the unloading strain reaches the failure point of the dry carbon FRCM specimens. After this point, the stiffness deteriorates faster for dry fabric up to $E_{re,i}/E_{re,0}$ of about 0.4, while cylinders confined with epoxy-coated fabric maintained a low deterioration ratio with minimum values between 0.6 and 0.7.

4 | CONCLUSIONS

The research work presented in this paper experimentally investigates the behavior of concrete confined through FRCM composites when exposed to moderately high temperatures; 150 × 300 mm ($d \times h$) concrete cylinders were confined using two types of FRCM jackets that have the same cementitious matrix but differ in the type of reinforcement embedded, one using dry (uncoated) and the other using ER-coated carbon fabric. Specimens were left curing for at least 90 days before being subjected to three temperature levels, being: 80°C, 100°C, and 250°C, in addition to the reference confined specimens maintained at standard ambient temperature (~20°C). The range of analyzed temperature extend the current research on the behavior of FRCM-confined concrete at high temperature. Specimens were tested using a compressive cyclic loading protocol, after a cooling down phase, and the experimental results in terms of compressive strength were compared to the theoretical ones computed using existing FRCM confinement models, that do not consider any temperature-correlated parameters. The results showed that:

- High temperature exposure significantly influences the overall axial stress–strain behavior of FRCM-confined specimens for both dry and epoxy-coated carbon fabrics,

mainly in terms of the type of stress–strain curve that can be displayed (hardening vs. plateau or softening).
- FRCM jackets with epoxy-coated carbon fabric performed better than the dry ones at all temperature steps considered in this study, both in terms of strength enhancement and axial strain capacity, probably due to the matrix–polymer interlocking occurring in the analyzed range of temperatures.
- A good axial ductility was maintained in all confined specimens, independently of the temperature exposure.
- High temperature exposure seems to have negligible effects on the cyclic unloading–reloading parameters as plastic strains and stiffness deterioration. A slight influence was observed for the stress deterioration coefficient for specimens subjected to 250°C.

AUTHOR CONTRIBUTIONS

Klajdi Toska: conceptualization; methodology; data curation; investigation; formal analysis; writing—original draft; visualization; writing—review and editing. **Flora Faleschini**: Conceptualization; methodology; investigation; resources; writing—review and editing; supervision; project administration. **Anne-Lise Beaucour**: Writing—review and editing; supervision; validation. **Carlo Pellegrino**: Writing–review and editing; supervision; validation. **Albert Noumowe**: Writing—review and editing; supervision; project administration.

ACKNOWLEDGMENTS

K.T. acknowledges funding from the H2020 Marie Skłodowska-Curie Actions and innovation Marie Skłodowska-Curie Actions, under grant agreement no. 945380.

Authors would like to thank G&P Intech for providing the FRCM materials. Eng. Daniela Foggetti is also acknowledged for her help during specimens' preparation.

CONFLICT OF INTEREST STATEMENT

The authors declare no conflicts of interest.

DATA AVAILABILITY STATEMENT

The data that support the findings of this study are available from the corresponding author upon reasonable request.

ORCID

Klajdi Toska https://orcid.org/0000-0002-4131-7683
Flora Faleschini https://orcid.org/0000-0003-2126-9300

REFERENCES

1. United Nations (2015) Resolution adopted by the General Assembly on 25 September 2015. 70/1. Transforming our world: the 2030 Agenda for Sustainable Development.
2. Donnini J, Spagnuolo S, Corinaldesi V. A comparison between the use of FRP, FRCM and HPM for concrete confinement. Compos Part B Eng. 2019;160:586–94. https://doi.org/10.1016/j.compositesb.2018.12.111
3. Papanicolaou CG, Triantafillou TC, Papathanasiou M, Karlos K. Textile reinforced mortar (TRM) versus FRP as strengthening material of URM walls: out-of-plane cyclic loading. Mater Struct. 2008;41(1):143–57. https://doi.org/10.1617/s11527-007-9226-0
4. Harajli M, ElKhatib H, San-Jose JT. Static and cyclic out-of-plane response of masonry walls strengthened using textile-mortar system. J Mater Civ Eng. 2010;22(11):1171–80. https://doi.org/10.1061/(ASCE)MT.1943-5533.0000128
5. Mazzotti C, Ferracuti B, Bellini A. Experimental bond tests on masonry panels strengthened by FRP. Compos Part B Eng. 2015;80:223–37. https://doi.org/10.1016/j.compositesb.2015.05.019
6. Tetta ZC, Bournas DA. TRM vs FRP jacketing in shear strengthening of concrete members subjected to high temperatures. Compos Part B Eng. 2016;106:190–205. https://doi.org/10.1016/j.compositesb.2016.09.026
7. Raoof SM, Bournas DA. Bond between TRM versus FRP composites and concrete at high temperatures. Compos Part B Eng. 2017;127:150–65. https://doi.org/10.1016/j.compositesb.2017.05.064
8. Bournas DA, Lontou PV, Papanicolaou CG, Triantafillou TC. Textile-reinforced mortar versus fiber-reinforced polymer confinement in reinforced concrete columns. ACI Struct J. 2007;104(6):740. https://doi.org/10.14359/18956
9. Toska K, Faleschini F. FRCM-confined concrete: monotonic vs. cyclic axial loading. Compos Struct. 2021;268:113931. https://doi.org/10.1016/j.compstruct.2021.113931
10. Toska K, Faleschini F, Zanini MA. Confinement of concrete with FRCM: influence of bond aspects under cyclic axial loading. Constr Build Mater. 2023;368:130432. https://doi.org/10.1016/j.conbuildmat.2023.130432
11. Toska K, Faleschini F, Zanini MA, Hofer L, Pellegrino C. Repair of severely damaged RC columns through FRCM composites. Constr Build Mater. 2021;273:121739. https://doi.org/10.1016/j.conbuildmat.2020.121739
12. Bournas DA, Triantafillou TC, Zygouris K, Stavropoulos F. Textile-reinforced mortar (TRM) versus FRP jacketing in seismic retrofitting of RC columns with continuous or lap-spliced de-formed bars. J Compos Constr. 2009;13(5):360–71. https://doi.org/10.1061/(ASCE)CC.1943-5614.0000028
13. Feng R, Li Y, Zhu JH, Xing F. Behavior of corroded circular RC columns strengthened by C-FRCM under cyclic loading. Eng Struct. 2021;226:111311. https://doi.org/10.1016/j.engstruct.2020.111311
14. Toska K, Hofer L, Faleschini F, Zanini MA, Pellegrino C. Seismic behavior of damaged RC columns repaired with FRCM composites. Eng Struct. 2022;262:114339. https://doi.org/10.1016/j.engstruct.2022.114339
15. Faleschini F, Gonzalez-Libreros J, Zanini MA, Hofer L, Sneed L, Pellegrino C. Repair of severely-damaged RC exterior beam-column joints with FRP and FRCM composites. Compos Struct. 2019;207:352–63. https://doi.org/10.1016/j.compstruct.2018.09.059
16. Peng GF, Huang ZS. Change in microstructure of hardened cement paste subjected to elevated temperatures. Constr Build Mater. 2008;22(4):593–9. https://doi.org/10.1016/j.conbuildmat.2006.11.002

17. Schneider U. Concrete at high temperatures—a general review. Fire Saf J. 1988;13(1):55–68. https://doi.org/10.1016/0379-7112(88)90033-1
18. Chan SYN, Peng GF, Anson M. Fire behavior of high-performance concrete made with silica fume at various moisture contents. ACI Mater J. 1999;96(3):405–9. https://doi.org/10.14359/640
19. Xing Z, Beaucour AL, Hebert R, Noumowe A, Ledesert B. Influence of the nature of aggregates on the behaviour of concrete subjected to elevated temperature. Cem Concr Res. 2011;41(4):392–402. https://doi.org/10.1016/j.cemconres.2011.01.005
20. Razafinjato RN, Beaucour AL, Hebert RL, Ledesert B, Bodet R, Noumowe A. High temperature behaviour of a wide petrographic range of siliceous and calcareous aggregates for concretes. Constr Build Mater. 2016;123:261–73. https://doi.org/10.1016/j.conbuildmat.2016.06.097
21. Laneyrie C, Beaucour AL, Green MF, Hebert RL, Ledesert B, Noumowe A. Influence of recycled coarse aggregates on normal and high performance concrete subjected to elevated temperatures. Constr Build Mater. 2016;111:368–78. https://doi.org/10.1016/j.conbuildmat.2016.02.056
22. Yermak N, Pliya P, Beaucour AL, Simon A, Noumowé A. Influence of steel and/or polypropylene fibres on the behaviour of concrete at high temperature: spalling, transfer and mechanical properties. Constr Build Mater. 2017;132:240–50. https://doi.org/10.1016/j.conbuildmat.2016.11.120
23. Cree D, Pliya P, Green MF, Noumowé A. Thermal behaviour of unstressed and stressed high strength concrete containing polypropylene fibers at elevated temperature. J Struct Fire Eng. 2017;8(4):402–17. https://doi.org/10.1108/JSFE-07-2016-0014
24. Noumowé A, Carré H, Daoud A, Toutanji H. High-strength self-compacting concrete exposed to fire test. J Mater Civ Eng. 2006;18(6):754–8. https://doi.org/10.1061/(ASCE)0899-1561(2006)18:6(754)
25. Consiglio Superiore dei Lavori Pubblici, Linea Guida per la identificazione, la qualificazione ed il controllo di accettazione di compositi fibrorinforzati a matrice inorganica (FRCM) da utilizzarsi per il consolidamento strutturale di costruzioni esistenti. 2018 (in Italian).
26. Messori M, Nobili A, Signorini C, Sola A. Effect of high temperature exposure on epoxy-coated glass textile reinforced mortar (GTRM) composites. Constr Build Mater. 2019;212:765–74. https://doi.org/10.1016/j.conbuildmat.2019.04.026
27. Donnini J, De Caso y Basalo F, Corinaldesi V, Lancioni G, Nanni A. Fabric-reinforced cementitious matrix behavior at high-temperature: experimental and numerical results. Compos Part B Eng. 2017;108:108–21. https://doi.org/10.1016/j.compositesb.2016.10.004
28. Tlaiji T, Vu XH, Ferrier E, Larbi AS. Thermomechanical behaviour and residual properties of textile reinforced concrete (TRC) subjected to elevated and high temperature loading: experimental and comparative study. Compos Part B Eng. 2018;144:99–110. https://doi.org/10.1016/j.compositesb.2018.02.022
29. Homoro O, Vu XH, Ferrier E. Experimental and analytical study of the thermo-mechanical behaviour of textile-reinforced concrete (TRC) at elevated temperatures: role of discontinuous short glass fibres. Constr Build Mater. 2018;190:645–63. https://doi.org/10.1016/j.conbuildmat.2018.09.142
30. Kapsalis P, Triantafillou T, Korda E, Van Hemelrijck D, Tysmans T. Tensile performance of textile-reinforced concrete after fire exposure: experimental investigation and analytical approach. J Compos Constr. 2022;26(1):04021067. https://doi.org/10.1061/(ASCE)CC.1943-5614.0001162
31. de Andrade Silva F, Butler M, Hempel S, Toledo Filho RD, Mechtcherine V. Effects of elevated temperatures on the interface properties of carbon textile-reinforced concrete. Cem Concr Compos. 2014;48:26–34. https://doi.org/10.1016/j.cemconcomp.2014.01.007
32. Bertolli V, Signorini C, Nobili A, D'Antino T. Influence of severe thermal preconditioning on the bond between carbon FRCM and masonry substrate: effect of textile pre-impregnation. Constr Build Mater. 2023;409:134028. https://doi.org/10.1016/j.conbuildmat.2023.134028
33. Kapsalis P, Tysmans T, Van Hemelrijck D, Triantafillou T. State-of-the-art review on experimental investigations of textile-reinforced concrete exposed to high temperatures. J Compos Sci. 2021;5(11):290. https://doi.org/10.3390/jcs5110290
34. Trapko T. The effect of high temperature on the performance of CFRP and FRCM confined concrete elements. Compos Part B Eng. 2013;54:138–45. https://doi.org/10.1016/j.compositesb.2013.05.016
35. Ombres L. Structural performances of thermally conditioned PBO FRCM confined concrete cylinders. Compos Struct. 2017;176:1096–106. https://doi.org/10.1016/j.compstruct.2017.06.026
36. Ombres L, Mazzuca P, Verre S. Effects of thermal conditioning at high temperatures on the response of concrete elements confined with a PBO-FRCM composite system. J Mater Civ Eng. 2022;34(1):04021413. https://doi.org/10.1061/(ASCE)MT.1943-5533.0004053
37. Cerniauskas G, Tetta Z, Bournas DA, Bisby LA. Concrete confinement with TRM versus FRP jackets at elevated temperatures. Mater Struct. 2020;53:1–14. https://doi.org/10.1617/s11527-020-01492-x
38. Talo R, Abed F, El Refai A, Alhoubi Y. Experimental investigation of concrete cylinders confined with PBO FRCM exposed to elevated temperatures. Fire. 2023;6(8):322. https://doi.org/10.3390/fire6080322
39. RILEM Technical Committees 129-MHT. Test methods for mechanical properties of concrete at high temperatures. Part 1: introduction. Part 2: stress–strain relation. Part 3: compressive strength for service and accident conditions. Mater Struct. 1995;28:410–4.
40. GP Intech. Rete in carbonio C-NET 170BL, Sch. Tec. FS06-170BL. 2021 (in Italian).
41. GP Intech. Rete in carbonio C-NET 220BL, Sch. Tec. FS06-220BL. 2021 (in Italian).
42. EN 1015-11. Methods of test for mortar for masonry – Part 11: determination of flexural and compressive strength of hardened mortar. Brussels, Belgium: Committee European de Normalisation; 2019.
43. Lam L, Teng JG. Design-oriented stress–strain model for FRP-confined concrete. Constr Build Mater. 2003;17(6–7):471–89. https://doi.org/10.1016/S0950-0618(03)00045-X
44. Toska K, Faleschini F. A new confinement model for FRCM confined concrete. Mater Struct. 2023;56(5):98. https://doi.org/10.1617/s11527-023-02186-w
45. Bamonte P, Gambarova PG. A study on the mechanical properties of self-compacting concrete at high temperature and after

cooling. Mater Struct. 2012;45:1375–87. https://doi.org/10.1617/s11527-012-9839-9
46. Ma Q, Guo R, Zhao Z, Lin Z, He K. Mechanical properties of concrete at high temperature—a review. Constr Build Mater. 2015; 93:371–83. https://doi.org/10.1016/j.conbuildmat.2015.05.131
47. Consiglio Nazionale delle Ricerche, CNR DT 215-2018. Istruzioni per la Progettazione, l'Esecuzione ed il Controllo di Interventi di Consolidamento Statico mediante l'utilizzo di Compositi Fibrorinforzati a Matrice Inorganica. 2018 (in Italian).
48. ACI549.4R-20. Guide to design and construction of externally bonded fabric-reinforced cementitious matrix (FRCM) and steel reinforced grout (SRG) systems for repair and strengthening concrete structures. 2020.
49. Triantafillou TC, Papanicolaou CG, Zissimopoulos P, Laourdekis T. Concrete confinement with textile-reinforced mortar jackets. ACI Struct J. 2006;103(1):28. https://doi.org/10.14359/15083
50. Ombres L, Mazzuca S. Confined concrete elements with cement-based composites: confinement effectiveness and prediction models. J Compos Constr. 2017;21(3):04016103. https://doi.org/10.1061/(ASCE)CC.1943-5614.0000755
51. Cascardi A, Longo F, Micelli F, Aiello MA. Compressive strength of confined column with fiber reinforced mortar (FRM): new design-oriented-models. Constr Build Mater. 2017; 156:387–401. https://doi.org/10.1016/j.conbuildmat.2017.09.004
52. Richart FE, Brandtzaeg A, Brown RL. A study of the failure of concrete under combined compressive stresses. Bulletin no. 185. Urbana, IL: University of Illinois, Engineering Experimental Station; 1928.
53. Lam L, Teng JG. Stress–strain model for FRP-confined concrete under cyclic axial compression. Eng Struct. 2009;31(2):308–21. https://doi.org/10.1016/j.engstruct.2008.08.014
54. Colajanni P, Fossetti M, Macaluso G. Effects of confinement level, cross-section shape and corner radius on the cyclic behavior of CFRCM confined concrete columns. Constr Build Mater. 2014;55: 379–89. https://doi.org/10.1016/j.conbuildmat.2014.01.035

AUTHOR BIOGRAPHIES

Klajdi Toska, Laboratoire de Mécanique & Matériaux du Génie Civil – L2MGC, CY Cergy Paris Université, 5 Mail Gay Lussac, 95000 Neuville-sur-Oise, France; CY Institute for Advanced Studies, 1 Rue Descartes, 95000 Neuville-sur-Oise, France. Email: klajdi.toska@cyu.fr

Flora Faleschini, Department of Civil, Environmental and Architectural Engineering, University of Padova, via Francesco Marzolo 9, Padova, Italy. Email: flora.faleschini@dicea.unipd.it

Anne-Lise Beaucour, Laboratoire de Mécanique & Matériaux du Génie Civil – L2MGC, CY Cergy Paris Université, 5 Mail Gay Lussac, 95000 Neuville-sur-Oise, France. Email: anne-lise.beaucour@cyu.fr

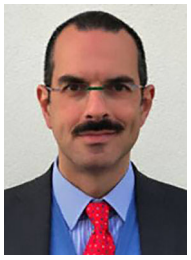

Carlo Pellegrino, Department of Civil, Environmental and Architectural Engineering, University of Padova, via Francesco Marzolo 9, Padova, Italy. Email: carlo.pellegrino@unipd.it

Albert Noumowe, Laboratoire de Mécanique & Matériaux du Génie Civil – L2MGC, CY Cergy Paris Université, 5 Mail Gay Lussac, 95000 Neuville-sur-Oise, France. Email: albert.noumowe@cyu.fr

How to cite this article: Toska K, Faleschini F, Beaucour A-L, Pellegrino C, Noumowe A. Effect of high temperature on FRCM-confined concrete. Structural Concrete. 2024. https://doi.org/10.1002/suco.202301022